THE JOURNAL OF PHYSICAL CHEMISTRY B

Article

pubs.acs.org/JPCB

Corrosion Stability and Bioactivity in Simulated Body Fluid of Silver/Hydroxyapatite and Silver/Hydroxyapatite/Lignin Coatings on Titanium Obtained by Electrophoretic Deposition

Sanja Eraković,[†] Ana Janković,[‡] Djordje Veljović,[†] Eriks Palcevskis,[§] Miodrag Mitrić,[∥] Tatjana Stevanović,[⊥] Djordje Janaćković,[†] and Vesna Mišković-Stanković*[,†]

[†]Faculty of Technology and Metallurgy, University of Belgrade, Karnegijeva 4, 11000 Belgrade, Serbia

[‡]Nanotechnology and Functional Materials Centre, Faculty of Technology and Metallurgy, University of Belgrade, Karnegijeva 4, 11000 Belgrade, Serbia

[§]Institute of Inorganic Chemistry, Riga Technical University, 34 Miera Street, Salaspils, LV-2169, Latvia

[∥]Vinča Institute of Nuclear Sciences, University of Belgrade, Mike Petrovića Alasa 12-14, 11000 Belgrade, Serbia

[⊥]Département des Sciences du Bois et de la Forêt, Université Laval, 2425 rue de la Terrasse, Québec, Canada

ABSTRACT: Hydroxyapatite is the most suitable biocompatible material for bone implant coatings. However, its brittleness is a major obstacle, and that is why, recently, research focused on creating composites with various biopolymers. In this study, hydroxyapatite coatings were modified with lignin in order to attain corrosion stability and surface porosity that enables osteogenesis. Incorporating silver, well known for its antimicrobial properties, seemed the best strategy for avoiding possible infections. The silver/hydroxyapatite (Ag/HAP) and silver/hydroxyapatite/lignin (Ag/HAP/Lig) coatings were cathaphoretically deposited on titanium from ethanol suspensions, sintered at 900 °C in Ar, and characterized by X-ray diffraction, scanning electron microscopy, field emission scanning electron microscopy, attenuated total reflection Fourier transform infrared, and X-ray photoelectron spectroscopy. The corrosion stability of electrodeposited coatings was evaluated in vitro in Kokubo's simulated body fluid (SBF) at 37 °C using electrochemical impedance spectroscopy. Bioactivity was estimated by immersion in SBF to evaluate the formation of hydroxyapatite on the coating surface. A microcrystalline structure of newly formed plate-shaped carbonate-hydroxyapatite was detected after only 7 days, indicating enhanced bioactive behavior. Both coatings had good corrosion stability during a prolonged immersion time. Among the two, the Ag/HAP/Lig coating had a homogeneous surface, less roughness, and low values of contact angle.

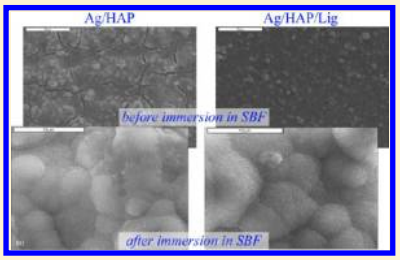

1. INTRODUCTION

Traditional biomedical metallic implants are irreplaceable in repairing the damaged bone tissue, but the greatest concern is their gradual electrochemical degradation.[1] The implants face a severe corrosion environment that includes blood and body fluid composed of several constituents (water, sodium, chlorine, proteins, plasma, and amino acids) along with mucin in the case of saliva. These metallic devices are unique in a way that they are exposed to living cells, tissues, and biological fluids, a dynamic, but also a hostile, environment for the preservation of the implant. Even though presently available bone implant materials exhibit high corrosion resistance, the body fluid environment inevitably results in the release of noncompatible metal ions by the implants into the body. The released ions are found to cause allergic and toxic reactions.

Titanium and its alloys have become the material of choice for long-term implant application for their favorable corrosion resistance as well as their low toxicity, biocompatibility, and good mechanical properties, such as high strength, durability, and light weight.[2−5] It has been well documented that Ti represents the most stable implant component with minimal effects on the surrounding body tissue involving inflammation, hypersensitivity, and allergic reactions.[1] Therefore, an ideal material for bone repair must be biocompatible and bioactive, able to initiate osteogenesis, and able to simulate the mechanical properties of bone with high corrosion resistance in the human body.[6]

To minimize direct metal−body fluid contact and to limit undesired metallic ions from being released into the body, biocompatible coatings on the metallic substrate, such as hydroxyapatite (HAP) [$Ca_{10}(PO_4)_6(OH)_2$], are suggested by many researchers.[2−8] Many in vivo studies have reported enhanced Ti implant fixation properties when coated with HAP.[5−7]

Postopt infections are the result of bacterial adhesion to the implant surface, and subsequently, biofilm forms at the implantation site.[9] To stop bacterial infection, it is crucial to inhibit bacterial adhesion since biofilm can be very resistant to

Special Issue: B: Electrophoretic Deposition

Received: May 30, 2012
Revised: September 4, 2012
Published: September 19, 2012

dx.doi.org/10.1021/jp305252a | J. Phys. Chem. B 2013, 117, 1633−1643

immune response and antibiotics.[10] The antimicrobial activity of silver and silver ions has been known for a very long time; additionally, the silver cation does not develop bacterial resistance and, at the same time, shows low toxicity to human cells.[11,12] Though the exact mechanism of Ag^+ action is not completely revealed, it is believed that it disrupts the function of bacterial cell membranes and binds to DNA and thiol groups in proteins. Therefore, the possibility to prevent the bone implant infections by using antimicrobial properties of Ag has generated great interest in the development of silver-doped HAP coatings.[13]

There are various methods to deposit ceramic coatings on metal surfaces, such as plasma spraying, sputtering, pulsed laser deposition, sol−gel, electrophoresis, and electrodeposition.[14] Among these, electrophoretic deposition (EPD) emerges as a method of choice due to its simple setup and formation of uniform coatings, even on substrates with complex shapes.[15−23] Other advantages are that EPD represents an inexpensive electrochemical technique that can be carried out at room temperature with the possibility of coating thickness and morphology well controlled by adjusting deposition parameters.

HAP coatings on metal implants show high biocompatibility and enhanced corrosion resistance but, on the other hand, exhibit poor adhesion properties due to their brittleness.[5] Specifically, the brittle nature of HAP can become a serious impediment during surgical operation or after implantation, since it does not provide the necessary mechanical stability of the interface between the coating and the titanium substrate. To improve the mechanical properties and adhesion and overcome the brittleness of HAP, our attention has been turned to engaging a biopolymer component into the HAP coating,[24,25] or even different synthetic polymers.[26,27] On the basis of recent research developments, organosolv lignin emerged as a suitable candidate for composite hydroxyapatite/polymer coatings. Lignin (Lig) is a complex natural polymer composed primarily of phenolic moieties connected with variety of chemical bonds.[28] Lignin possesses antioxidant and antimicrobial properties; therefore, its incorporation is interesting in medical applications because of its thermal stability and biocompatibility in different materials.[29−31] Additionally, Martinez et al.[30] have shown that the hydroxyapatite/lignin scaffold integrates well into the bone tissue, which can recommend it as a biocompatible and oseoconductor substitute in the case of bone damage. Our assumption was that organosolv lignin will help in providing a more stable composite in order to accommodate a better interconnected porous structure. It is our belief that lignin can help diminish the severe cracking of HAP coatings, as reported by Wang et al.,[32] for the composite with chitosan.

The aim of this research is to investigate the corrosion stability and bioactivity of silver/hydroxyapatite and silver/hydroxyapatite/lignin coatings electrodeposited on titanium in Kokubo's simulated body fluid (SBF).

2. EXPERIMENTAL SECTION

2.1. Synthesis of Hydroxyapatite Powder Doped with Ag. A modified chemical precipitation method was used to prepare silver/hydroxyapatite powder by the reaction of calcium oxide (obtained by calcination of $CaCO_3$ for 5 h at 1000 °C in air), silver nitrate, and phosphoric acid. A stoichiometric amount of the resulting calcium oxide was mixed and stirred in distilled water for 10 min; afterward, $AgNO_3$ solution was added to the suspension, yielding a final concentration of silver ion of 0.4 ± 0.1 wt %. Finally, phosphoric acid was added dropwise to the suspension in order to obtain silver/hydroxyapatite powder, $Ca_{9.95}Ag_{0.05}(PO_4)_6(OH)_2$. When all the necessary quantity of phosphoric acid was introduced, the pH reached a value of 7.4−7.6. The obtained suspension was preheated to 94 ± 1 °C for 30 min and stirred for another half an hour. After sedimentation, the upper clear solution layer was decanted. The suspension was then spray-dried at 120 ± 5 °C into granulated powder.

2.2. Particle Size Distribution and ζ-Potential. An absolute ethanol Ag/HAP suspension (total volume = 100 mL) was prepared by dissolving 1.0034 g of nanosized Ag/HAP powder. In the case of the Ag/HAP/Lig suspension, an additional 0.01 g of lignin was added to the final volume. Subsequently, solutions were sonicated for 15 min to obtain homogeneous and stable suspensions. To increase the stability of the suspension, HCl was added until the pH value of 2.00 was reached. Prior to electrodeposition, the ethanol Ag/HAP and Ag/HAP/Lig suspensions were ultrasonically treated for 30 min to obtain a homogeneous suspension. The Ag/HAP and Ag/HAP/Lig particle size distribution and zeta potential, ζ, were determined using a Zeta-Sizer Nano ZS with a 633 nm He−Ne laser (Malvern, U.K.). The instrument can measure particle sizes ranging from 0.6 nm to 6 μm.

2.3. Surface Preparation of Titanium. The titanium plates (dimensions: 25 mm × 10 mm × 0.25 mm, for surface analysis; 40 mm × 20 mm × 0.25 mm, for impedance measurements; Aldrich, purity = 99.7%) were used as metal substrates for cathodic deposition of Ag/HAP and Ag/HAP/Lig coatings. Before deposition, Ti plates were mechanically pretreated. First, metal plates were polished with grit emery paper, followed by wet polishing with 0.3 μm alumina. Afterward, plates were degreased in acetone and then in ethanol for 15 min in an ultrasonic bath.

2.4. Electrophoretic Deposition of Ag/HAP and Ag/HAP/Lig Coatings on Titanium. Lignin powder was used to produce the biocomposite silver/hydroxyapatite/lignin coating. Alcell lignin from Repap Enterprises Inc. (Stamford, CT) was used without further purification. Alcell lignin was derived from pulping of a mixture of hardwoods (maple, birch, and poplar) by an organosolv process using aqueous ethanol, which explains its solubility in ethanol, an important property for the present study.

Electrophoretic deposition was performed from ethanol suspensions previously described in section 2.2. Prior to electrodeposition, the Ag/HAP and Ag/HAP/Lig suspensions were ultrasonically treated for 30 min to obtain a homogeneous particle distribution.

A three-electrode cell arrangement was used for cathodic electrodeposition. The working electrode was a titanium plate, and the counter electrodes were two platinum panels, placed parallel to the working electrode at a distance of 1.5 cm. The coatings were deposited from ethanol Ag/HAP and Ag/HAP/Lig suspensions, using the constant voltage method. The experiments were performed at 60 V for a deposition time of 45 s, at room temperature.

Electrodeposited Ag/HAP and Ag/HAP/Lig coatings were air-dried for 24 h at room temperature. Afterward, the coatings were sintered at 900 °C for 30 min in an argon atmosphere, with the initial heating rate of 16 °C/min. Before sintering, the oxygen was eliminated from coatings in an argon atmosphere at 200 °C for 45 min.

dx.doi.org/10.1021/jp305252a | J. Phys. Chem. B 2013, 117, 1633−1643

2.5. Characterization Methods. *2.5.1. Contact Angle Measurements.* The contact angle measurements were used to evaluate the hydrophilic or hydrophobic balance—wettability of electrophoretic Ag/HAP and Ag/HAP/Lig coatings by using a dynamic contact angle analyzer, a FTA 200 Angle Meter (Goniometre Folio Instruments, Inc.), in sessile drop mode. The simulated body fluid (SBF) at pH 7.4 was used to investigate the wettability of samples with 6 μL sessile volume drops. The drop image was recorded using a videocamera.

2.5.2. Surface Roughness. The surface roughness of Ag/HAP and Ag/HAP/Lig coatings cataphoretically deposited on titanium was determined by a TR-200 hand-held rougness tester.

2.5.3. X-Ray Diffraction. The phase composition of electrodeposited coatings were investigated by X-ray diffraction (XRD) using a Philips PW 1051 powder diffractometer with Ni-filtered Cu Kα radiation (λ = 1.5418 Å). The diffraction intensity was measured by using the scan-step technique in the range of 2θ = 8−80°, a scanning step width of 0.05°, and an exposition time of 50 s per step. The phase analysis was done by using the PDF-2 database with a commercially available computer program, EVA V.9.0.

The mean crystallite domain size (D_p) was calculated from the half-height width ($\beta_{1/2}$) of the XRD reflection of the (002) plane (at 2θ = 25.8°), using the Scherrer equation (eq1)

$$D_p = \frac{K\lambda}{\beta_{1/2}\cos\theta} \quad (1)$$

where λ is the wavelength of the X-ray radiation, K is the shape coefficient equal to 0.9, and θ is the diffraction angle.

2.5.4. Scanning Electron Microscopy and Field Emission Scanning Electron Microscopy. A scanning electron microscope (SEM), a JEOL JSM-5800, and a field emission scanning electron microscope (FE-SEM), a TESCAN MIRA 3 XMU, operated at 20 keV, were used to analyze the morphology of the electrodeposited coatings, before and after immersion in SBF solution.

2.5.5. Attenuated Total Reflection Fourier Transform Infrared Spectroscopy. Attenuated total reflection Fourier transform infrared (ATR-FTIR) measurements were carried out with a Spectrum 400 PerkinElmer infrared spectrometer in the wavenumber of 600−4000 cm^{-1} in order to investigate the functional groups present in electrodeposited coatings before and after immersion in SBF solution.

2.5.6. X-ray Photoelectron Spectroscopy. X-ray photoelectron spectroscopy (XPS) as a surface chemical analysis of sintered Ag/HAP and Ag/HAP/Lig coatings was performed with an Axis-Ultra spectrometer (Kratos) using non- and monochromatized Al Kα radiation (1486.6 eV) and a hemispherical analyzer. The XPS spectra were background-subtracted, using the nonlinear, iterative Shirley method. Peak fitting was processed with CasaXPS, which automatically and iteratively minimizes the difference between the experimental spectrum and the calculated envelope by varying the parameters supplied in a first guess. The fitting procedure allowed signals to be evaluated by determining the peak position, height, width, and Gaussian/Lorentzian ratio.

2.5.7. Electrochemical Impedance Spectroscopy. For electrochemical impedance spectroscopy (EIS) measurements, electrodeposited Ag/HAP and Ag/HAP/Lig coatings and bare titanium, thermally treated, were exposed to SBF solution at a temperature of 37 °C for 10 days. A three-electrode cell arrangement was used in the experiments. The SBF solution (Table 1) was prepared by dissolving the reagent-grade salts

Table 1. Chemical Composition of Simulated Body Fluid (SBF)

reagents	c (g l^{-1})
NaCl	7.996
$NaHCO_3$	0.350
KCl	0.224
$K_2HPO_4{\cdot}3H_2O$	0.228
$MgCl_2{\cdot}2H_2O$	0.305
$CaCl_2$	0.278
Na_2SO_4	0.071
$(CH_2OH)_3CNH_2$	6.057
1 M HCl	40 mL

NaCl, $NaHCO_3$, KCl, $K_2HPO_4{\cdot}3H_2O$, $MgCl_2{\cdot}2H_2O$, $CaCl_2$, and Na_2SO_4 in deionized water and buffered in tris-hydroxymethyl aminomethane, pH adjusted to 7.40 with 1 M hydrochloric acid, at 37 °C. The working electrode was coated titanium or thermally treated bare titanium (tested surface area of 1 cm^2), the counter electrode was a platinum mesh, and the reference electrode was a saturated calomel electrode (SCE). The impedance data were obtained at the open-circuit potential using a Reference 600 Potentiostat/Galvanostat/ZRA (Gamry Instruments, Inc., Warminister, PA), over a frequency range of 300 kHz to 10 mHz using a 5 mV amplitude of sinusoidal voltage. The impedance spectra were analyzed using the Gamry Instruments Echem Analyst fitting program, version 5.50.

2.5.8. In Vitro Bioactivity. The bioactivity of Ag/HAP and Ag/HAP/Lig coatings was tested by immersion in 10 mL of SBF solution (Table 1), which was refreshed every 24 h. After 7 days, the samples were taken out, rinsed in deionized water and then air-dried before characterization by FE SEM, SEM, XRD, and ATR-FTIR analysis.

3. RESULTS AND DISCUSSION

3.1. Particle Size Distribution and ζ-Potential. The size distribution of particles and the value of the ζ-potential were investigated in order to obtain information that allows predictions about the stability of the colloidal systems.

The particle size distribution (PSD) measurement of Ag/HAP and Ag/HAP/Lig suspensions was made by using the dynamic light-scattering technique. The obtained average particle size is around 200 nm for both suspensions, although agglomerate peaks can be observed also, meaning that silver does not affect the Ag/HAP and Ag/HAP/Lig particle size.

The ζ-potential is a measure of the strength of interactions between colloid particles, and hence it relates to colloid solution stability. A biomaterial's ζ-potential indicates its electric surface properties. Bioceramic particles have to be electrically charged in order to be electrophoretically deposited on metal substrates.[33] As a result, the ζ-potential is an important factor to establish a stable suspension for electrophoretic deposition.[34] It is well known that the issue of the stability of disperse systems is essential for accomplishing the electrophoretic deposition. A cathaphoretic deposition assumes a positive ζ-potential of the particle surface during the whole process, which can certainly be achieved at a lower pH value.

High positive values of ζ-potential of 23 and 29 mV indicate positively charged particle surfaces of Ag/HAP and Ag/HAP/Lig, respectively, thus enabling the attraction of particles by a

dx.doi.org/10.1021/jp305252a | J. Phys. Chem. B 2013, 117, 1633−1643

negatively charged cathode−titanium plate and, therefore, successful electrophoretic deposition of coatings.

3.2. Contact Angle and Surface Roughness. The contact angle value, as an indicator of surface wettability and its biocompatibility, was determined by sessile drops of SBF solution on coating surfaces. The drop shapes of SBF on Ag/HAP and Ag/HAP/Lig coating surfaces are shown in Figure 1a,b, respectively. Measured contact angles at Ag/HAP and Ag/HAP/Lig coatings on Ti substrates were 35.03° ± 8.07° and 39.19° ± 1.21°, respectively. Surface wettability (hydrophobicity or hydrophilicity) is one of the most important parameters affecting biological response to implanted biomaterials. Wettability affects protein adsorption, platelet adhesion/activation, blood coagulation, and cell adhesion.[35] HAP is considered to be hydrophilic due to its −OH groups displayed on the surface.[36]

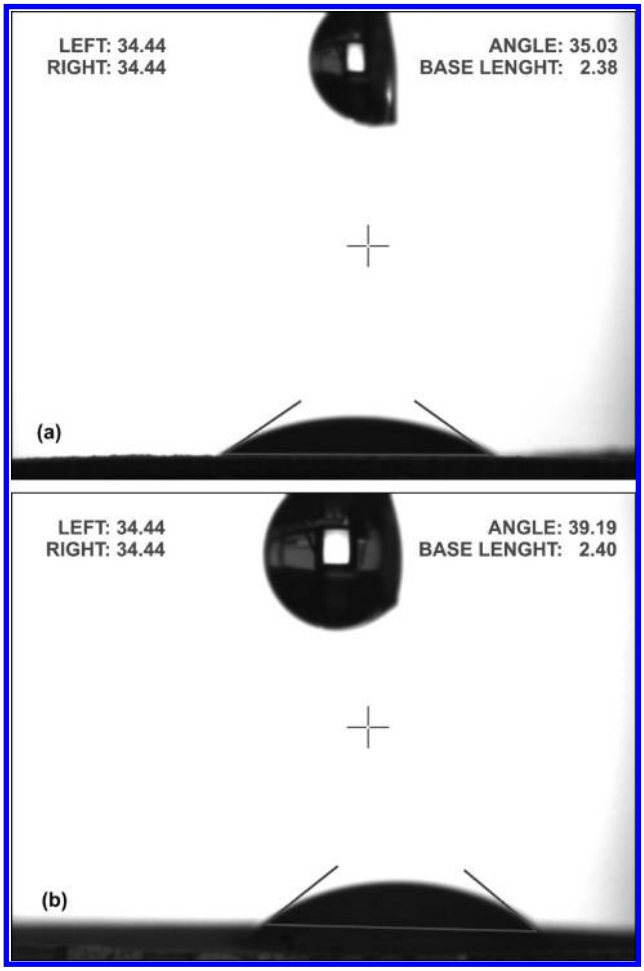

Figure 1. Contact angle measurements of SBF solution at the surface of (a) Ag/HAP and (b) Ag/HAP/Lig coatings on titanium.

A low contact angle is usually favorable in order to achieve high surface coverage. From Figure 1, it can be noticed that both coatings exhibit good hydrophilic properties. Hydrophilic surfaces were shown to promote the highest levels of cell attachment.[37]

The measured surface roughness values, R_a, of Ag/HAP and Ag/HAP/Lig coatings were 2.40 and 0.85 μm, respectively. Costa-Rodrigues et al.[38] reported that the surface roughness values of biomaterial ranging from 0.20 to 2.87 μm enhance the maximum osteoclastic development, thus directly affecting the cell adhesion. Reported R_a values[38] were in good agreement with our results. The same authors concluded that, even though rougher surfaces are better for cell adhesion, at the same time, they could become a problem for cellular mobility. Therefore, the surface roughness of the Ag/HAP/Lig coating could stimulate cellular response better than the Ag/HAP coating.

3.3. XRD Analysis. X-ray diffraction analysis was performed to determine the phase composition and structure of Ag/HAP and Ag/HAP/Lig coatings, presented in Figure 2a,b, respectively, before and after 7 days of immersion in SBF solution at 37 °C. As a comparison, the XRD spectrum of the pure HAP coating is shown in Figure 2a as well.[31] Labeled XRD peaks match very well to the JCPDS standard XRD card No. 86-1199 for hydroxyapatite, but incorporation of Ag in the hydroxyapatite crystal lattice causes a shift of specific HAP peaks to the left, confirming the silver substitution for calcium. The evidence of the presence of Ag was verified through the shift of characteristic HAP peaks (crystal planes (002), (211), (112), and (300)) toward smaller angles for the Ag/HAP coating before immersion in SBF solution compared with the pure HAP coating (Figure 2a).

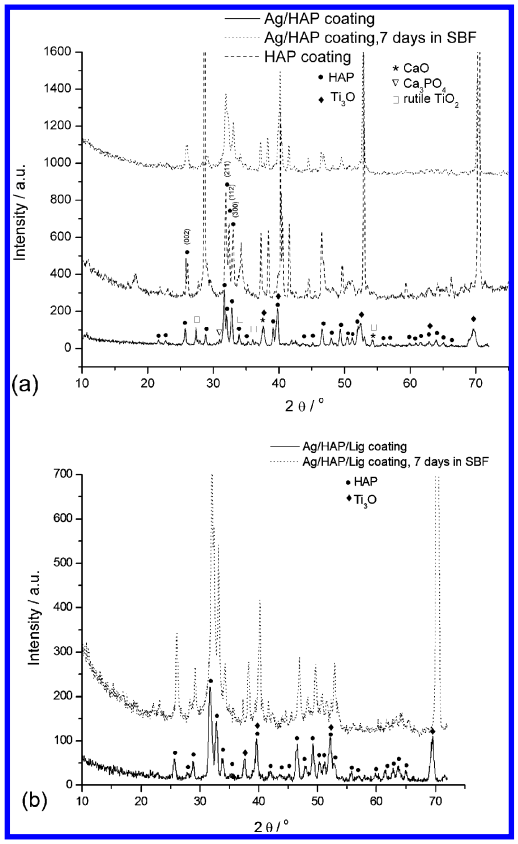

Figure 2. XRD patterns of (a) HAP and Ag/HAP and (b) Ag/HAP/Lig coatings, before and after 7 days of immersion in SBF solution at 37 °C.

The appearance of new peaks in the XRD pattern of the Ag/HAP coating, as one can see in Figure 4a, indicates the partial HAP decomposition. Although, the diffractogram of the Ag/HAP coating corresponds mainly to hydroxyapatite, the observed new diffraction peaks suggested the formation of crystalline phases, such as CaO (JCPDS No. 74-1226) and β-tricalcium phosphate (β-TCP, JCPDS No. 32-0176) at 2θ = 30.7°, confirming the slight decomposition of HAP during the

dx.doi.org/10.1021/jp305252a | J. Phys. Chem. B 2013, 117, 1633−1643

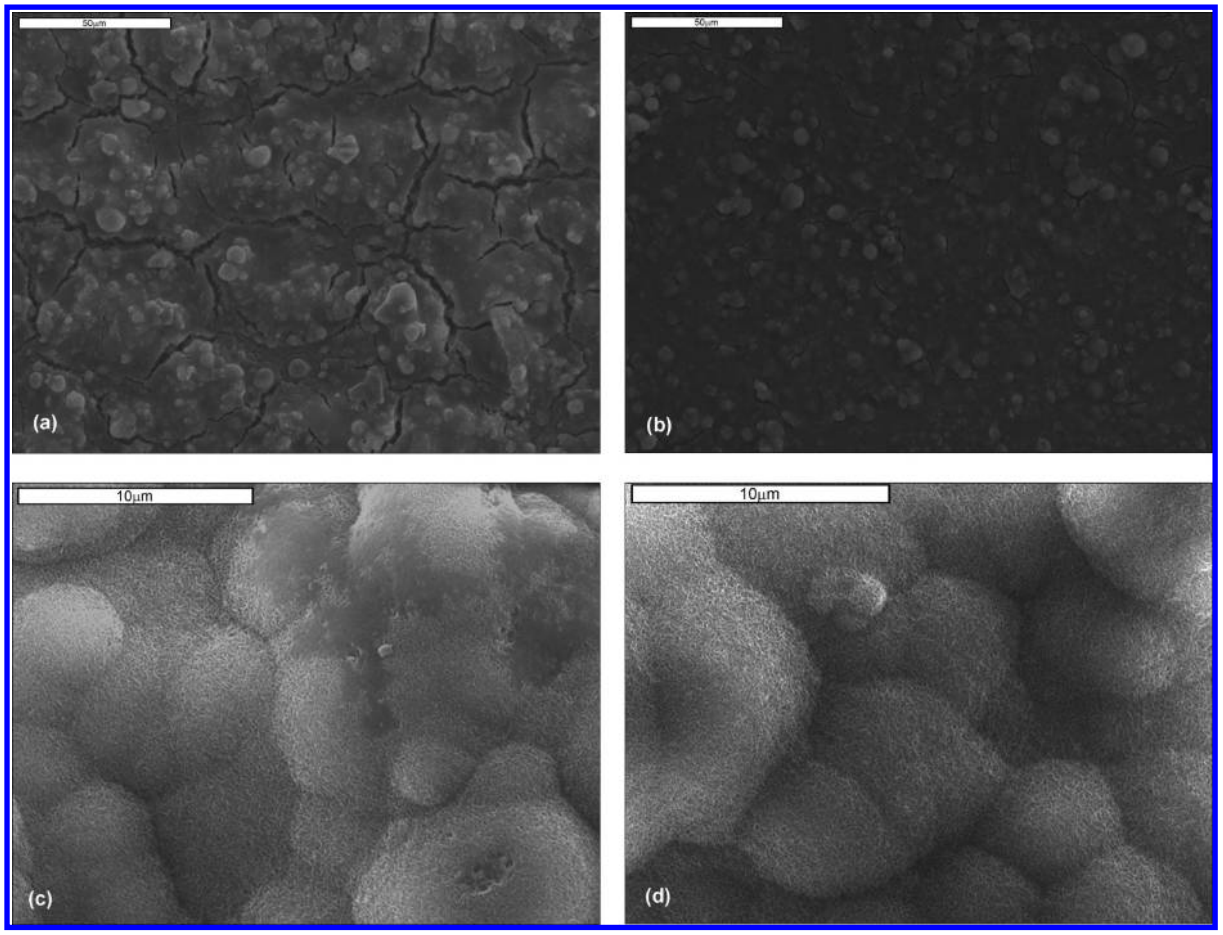

Figure 3. SEM microphotographs of the Ag/HAP coating (a) before and (c) after immersion and the Ag/HAP/Lig coating (b) before and (d) after immersion in SBF solution at 37 °C.

sintering process. On the other hand, the absence of the specific diffraction peaks for β-TCP and CaO in the XRD pattern of the Ag/HAP/Lig coating (Figure 2b) confirmed that no partial HAP decomposition occurred. Thus, all peaks matched pure hydroxyapatite. That led us to the conclusion that lignin improved the thermal stability of the Ag/HAP lattice during sintering.

The additional peaks in Figure 2a that originate from the Ti substrate indicate the presence of rutile TiO_2, although the sample was sintered in an inert atmosphere. Also, the suboxide of titanium, Ti_3O (JCPDS No. 73-1586), was detected in XRD patterns of both Ag/HAP and Ag/HAP/Lig coatings (Figure 2a,b), which is classified as a nonstoichiometric oxide deficient in oxygen. The complex valence status of Ti appears to be due to the oxygen diffusion from the exterior surface to the inside during sintering. According to Ye at al.,[39] Ti metal and Ti suboxides on the composite surfaces are believed to be more active than TiO_2 in the physiological environment and can activate chemical bonding between the implant surface and adjacent biomolecules.

SBF is known to be a metastable buffer solution like human plasma.[40] The formation of a bonelike apatite layer on the surface of bioactive materials has been reported after soaking these materials in a biomimetic system such as SBF solution. After 7 days of immersion in SBF solution, it is important to note the shift in characteristic hydroxyapatite peaks for both Ag/HAP and Ag/HAP/Lig coatings toward higher angles (Figure 2a,b). Those findings were attributed to carbonate ions in the lattice and confirmed, therefore, the growth of carbonate hydroxyapatite onto the coating surface. Therefore, the shifting of XRD diffraction peaks is typical for weak crystalline, carbonated HAP, as it is found in bone.

The crystallite domain sizes, calculated at $2\theta \approx 26°$ by the Scherrer equation (eq 1), for Ag/HAP and Ag/HAP/Lig coatings were 35.2 and 20.8 nm, respectively. On the other hand, the apatite layer obtained after 7 days of soaking in SBF had almost the same crystallite domain size on the Ag/HAP coating (20.2 nm) and the Ag/HAP/Lig coating (22.0 nm). The difference between the crystallite size before and after immersion is probably due to the incorporation of CO_3^{2-} ions into the apatite lattice by occupying the OH^- sites or the PO_4^{3-} position.[41]

3.4. SEM and FE-SEM Analysis. The surface morphologies of Ag/HAP and Ag/HAP/Lig coatings before and after 7 days of immersion in SBF at 37 °C are shown in Figure 3a–d, respectively. Also, the FE-SEM microphotograph of the Ag/HAP/Lig coating before and after immersion in SBF is presented in Figure 4.

The crystallite domain size of Ag/HAP/Lig coatings before and after soaking in SBF was calculated to be almost the same, 20.8 and 22.0 nm, respectively, indicating the homogeneous surface (Figure 3b,d). On the contrary, the crystallite domain size of Ag/HAP coatings before and after soaking in SBF was calculated to be 35.2 and 20.2 nm, respectively, revealing the decrease in crystallite domain size after soaking and a fractured surface (Figure 3a,c).

dx.doi.org/10.1021/jp305252a | J. Phys. Chem. B 2013, 117, 1633–1643

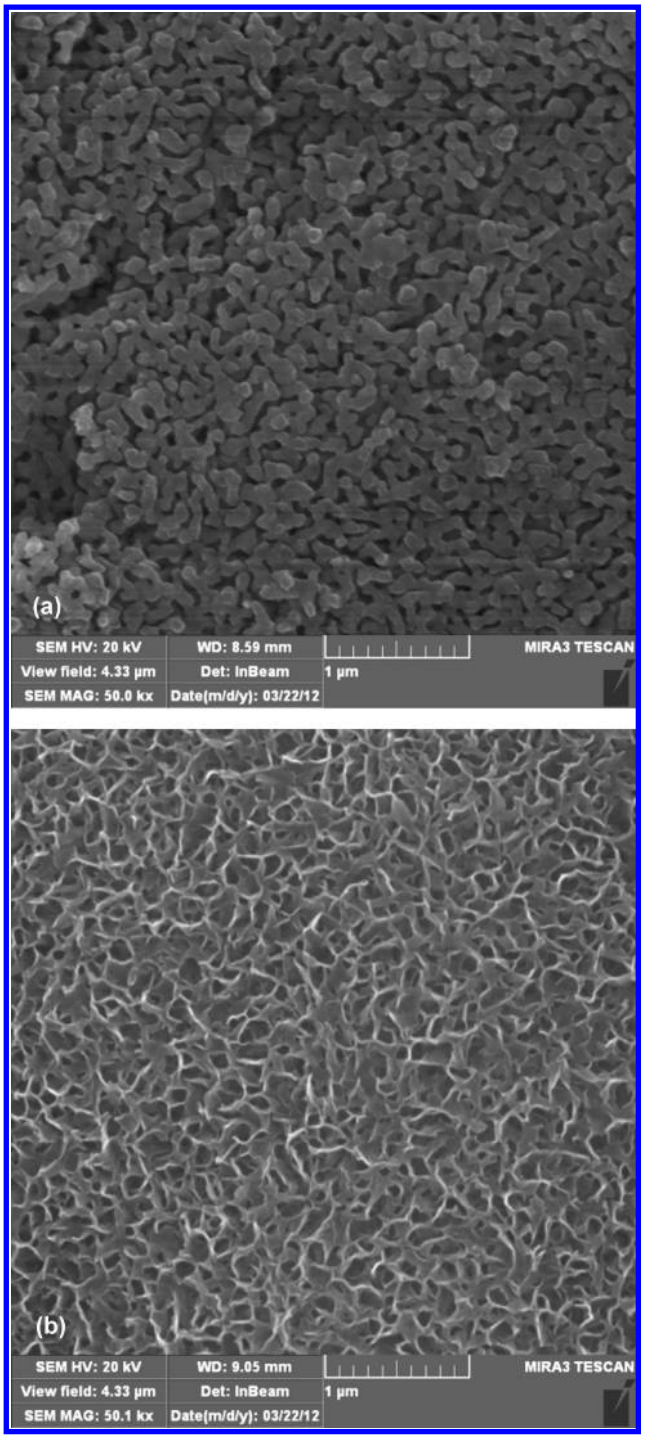

Figure 4. FE-SEM microstructure of the sintered Ag/HAP/Lig coating (a) before and (b) after 7 days of immersion in SBF solution at 37 °C.

The FE-SEM microphotograph in Figure 4a confirms the porous structure of the Ag/HAP/Lig coating surface, and the calculated grain size was 100 nm, whereas Figure 4b shows the FE-SEM image of the same sample with a newly formed apatite layer after soaking in SBF solution containing plate-shaped HAP crystals with high magnification (50 000×). Also, the observed high porosity is beneficial for better cell adhesion, as it enables better connection between the implant and the bone. It has been reported that open interconnected porosity structures facilitate penetration of the surrounding bone tissue and hence lead to better biointegration and mechanical stability.[3]

It is obvious that both Ag/HAP and Ag/HAP/Lig coatings formed an apatite film on the surface after just 7 days of immersion in SBF, indicating their potential bioactivity. The apatite composition of newly formed crystals was confirmed by XRD (Figure 2) and ATR-FTIR results (Figure 5, which will be discussed later), while the formation of apatite can be explained as follows.

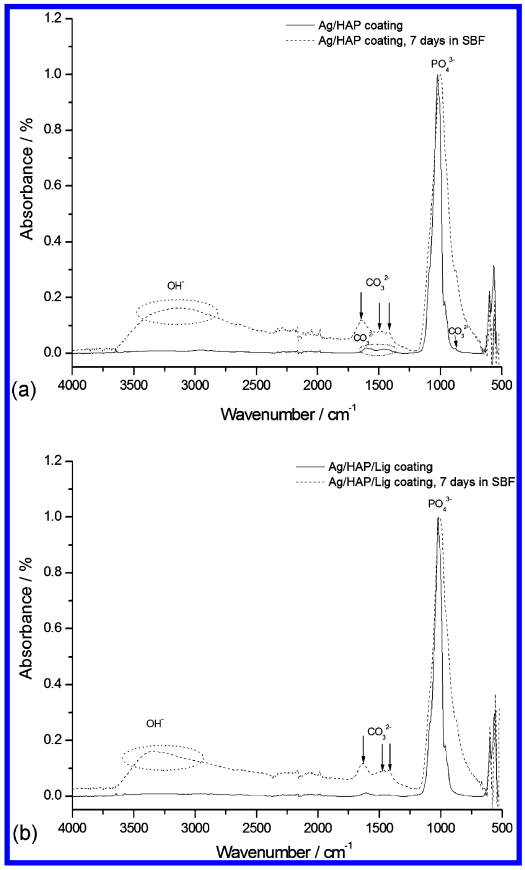

Figure 5. ATR-FTIR spectra of (a) Ag/HAP and (b) Ag/HAP/Lig coatings, before and after 7 days of immersion in SBF at 37 °C.

The HAP surface exhibited a negative charge that specifically interacted with the positive calcium ions from SBF, forming an amorphous Ca-rich apatite. The Ca-rich positively charged surface then interacted with the negative phosphate ions in the SBF to form Ca-poor apatite, which gradually crystallizes into bonelike apatite, through which the HAP appeared to stabilize in SBF. Once formed in SBF, the apatite grows spontaneously, consuming the calcium and phosphate ions, incorporating minor ions, such as sodium, magnesium, and carbonate, and thereby developing a bone mineral-like compositional and structural feature.[42]

3.5. ATR-FTIR Spectroscopy. The bioactivity of implanted apatite materials can be evaluated by the formation of bonelike apatite on their surface. The presence of carbonate bands in FTIR spectra is clear evidence of its incorporation in the surface of the HAP layer. It is known that the biological hydroxyapatite also contains carbonate groups.[43] Thus, the Ag/HAP and Ag/HAP/Lig coatings were investigated by the FTIR technique after immersion in SBF.

The FTIR spectra of Ag/HAP and Ag/HAP/Lig coatings are presented in Figure 5a,b, respectively. The FTIR spectra of Ag/HAP and Ag/HAP/Lig coatings before immersion in SBF

dx.doi.org/10.1021/jp305252a | J. Phys. Chem. B 2013, 117, 1633−1643

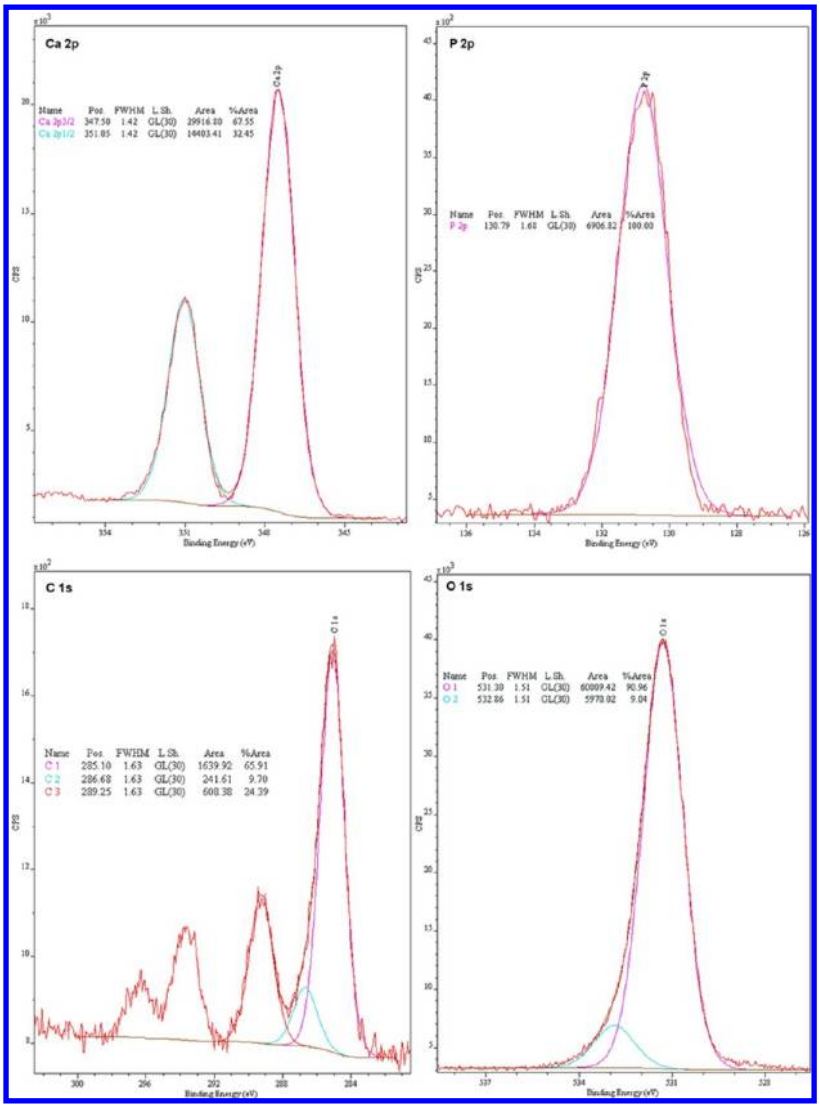

Figure 6. Deconvoluted XPS photoelectron lines of component elements (Ca, P, C, and O) for the Ag/HAP coating.

exhibit the typical bands for hydroxyapatite. The broad peak at 3432 cm^{-1} is related to H_2O adsorption. The three characteristic bands at 960, 1016, and 1089 cm^{-1} belong to vibration of the PO_4^{3-} group. Also, the weak characteristic bands at around 3573 and 627 cm^{-1} correspond to the vibration of structural OH^- groups in the hydroxyapatite.

Finally, in FTIR spectrum of Ag/HAP before immersion in SBF solution (Figure 5a), we noticed a very low-intensity wide band centered around 1400−1585 cm^{-1}, which may be attributed to carbonates (CO_3^{2-}).[43] The appearance of a small vibrational band at 875 cm^{-1} also indicates a trace amount of carbonates as a confirmation of Ag/HAP partial decomposition. Although the carbonates were not detected by XRD results, these peaks in the FTIR spectrum can be attributed to the reaction between CaO, confirmed in the XRD pattern (Figure 2a), and CO_2 from the atmosphere.[44] On the other hand, the absence of a low-intensity wide band (1400−1585 cm^{-1}) in the FTIR sprectrum of Ag/HAP/Lig before immersion in SBF solution (Figure 5b) confirmed that there was no decomposition of hydroxyapatite, as detected also by XRD (Figure 2b).

During 7 days of immersion in SBF at 37 °C, carbonated apatite was formed on the surface of coatings, as revealed by ATR-FTIR analysis. In biological apatite, some PO_4^{3-} ions are substituted by CO_3^{2-} ions. As a sensitive technique, IR can detect even a trace amount of carbonate.[45] FTIR spectra of the Ag/HAP and Ag/HAP/Lig coatings after 7 days of immersion in SBF solution (Figure 5a,b, respectively) revealed the broad absorbance at 3382 cm^{-1} attributed to the −OH stretching mode, and the intensity of the −OH band was observed to be higher for coatings after immersion, indicating newly formed bonelike apatite on the coating surface.[46] Also, another confirmation was triplet peaks at 1640, 1476, and 1420 cm^{-1} attributed to CO_3^{2-}, which belong to the vibrational bands of CO_3^{2-} groups of B-type carbonated apatite owing to the formation of bonelike apatite after soaking in SBF solution.[47] The spectrum of bonelike apatite showed a high concentration of hydroxyl and phosphate groups compared to peaks appearing in spectra obtained for coatings before immersion in SBF (Figure 5a,b), which makes the surface of coatings exhibit negative surface potentials required for apatite nucleation. Therefore, FTIR results indicate the bioactivity of both coatings and that their surfaces represent favorable substrates for apatite nucleation, which was also confirmed by SEM and FE-SEM pictures (Figures 3 and 4). The growth of

dx.doi.org/10.1021/jp305252a | J. Phys. Chem. B 2013, 117, 1633−1643

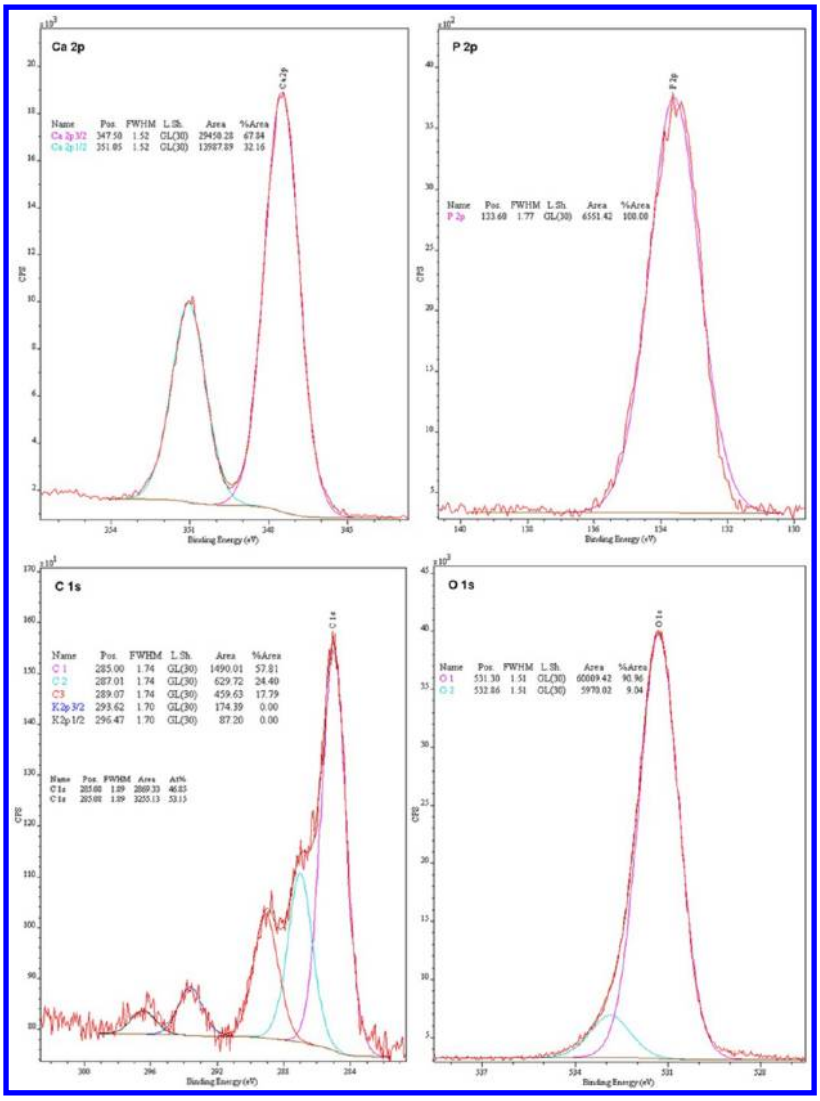

Figure 7. Deconvoluted XPS photoelectron lines of component elements (Ca, P, C, and O) for the Ag/HAP/Lig coating.

the apatite layer confirmed by our results resembled the structure of biological carbonated HAP.[40]

3.6. XPS Analysis. The XPS method offers the possibility of distinguishing between different types of chemical bonds of surface atoms on the basis of the chemical shift and change in shape of the XPS peaks.[26]

The survey spectra (0−1400 eV) and the high-resolution spectra of the C 1s, O 1s, P 2p, Ca 2p, and Ti 2p were obtained (Figures 6 and 7), whereas Ag could not be traced. Although, XPS is a very sensitive technique, this property applies only at the surface level. The evidence of the presence of Ag was verified through analysis of XRD spectra comparing HAP and Ag/HAP before immersion in SBF (Figure 2a), which is thoroughly discussed in section 3.3.

Surface analysis of Ag/HAP and Ag/HAP/Lig coatings before soaking in SBF performed by XPS are illustrated in Figures 6 and 7, respectively. The measured binding energy values were calibrated by the C 1s (hydrocarbon C−C, C−H) of 285 eV. Deconvoluted spectra corresponding to different elements (Ca, P, and O) are discussed. The relative concentrations of most prominent elements and XPS transitions (C 1s, O 1s, Ca 2p, P 2p) for Ag/HAP and Ag/HAP/Lig coatings are presented in Table 2.

Table 2. Atomic Percentages and Ca/P Ratio at Sample Surface of Ag/HAP and Ag/HAP/Lig Coatings Determined by XPS

	element				
sample	C 1s (%)	O 1s (%)	Ca $2p_{3/2}$ (%)	P 2p (%)	Ca/P
Ag/HAP	6.9	62.0	19.1	11.2	1.70
Ag/HAP/Lig	5.8	62.3	18.7	11.5	1.62

Figures 6 and 7 show the deconvolution XPS spectra of C 1s, O 1s, Ca 2p, and P 2p core-level spectra of Ag/HAP and Ag/HAP/Lig coatings. From both XPS spectra, the Ca 2p spectrum of the coatings reveals a doublet with Ca $2p_{3/2}$ (BE of 347.5 eV) and Ca $2p_{1/2}$ (BE of 351.1 eV), and the P 2p spectrum of the coating reveals a single P $2p_{3/2}$ peak at the BE position at 133.6 eV, for the Ag/HAP coating (Figure 6), and 133.8 eV, for the Ag/HAP/Lig coating (Figure 7), indicating the presence of hydroxyapatite,[48,49] but no Ag peak was detected in XPS spectra because the amount of doped silver in the crystal lattice of HAP is very small.

Although the Ca 2p spectrum of the Ag/HAP coating shows a doublet of Ca $2p_{3/2}$ and Ca $2p_{1/2}$ with the same binding energies as those for Ag/HAP/Lig coatings, according to the

dx.doi.org/10.1021/jp305252a | J. Phys. Chem. B 2013, 117, 1633−1643

literature,[49] Ca $2p_{3/2}$ and Ca $2p_{1/2}$ (347.5 and 351.1 eV, respectively) can also correspond to Ca 2p in $Ca_3(PO_4)_2$ and $Ca_{10}(PO_4)_6(OH)_2$. These transitions for Ca 2p make differentiation between chemical environments impossible to identify with outmost certainty by XPS analysis alone. The Ca might exist in various phases, such as CaO and $Ca_3(PO_4)_2$ that occur during hydroxyapatite sintering. These results can confirm HAP decomposition after sintering the Ag/HAP coating, which was also indicated by XRD analysis (Figure 2a) and ATR-FTIR measurement (Figure 5a).

The main O 1s peak component at BE = 531.3 eV for both coatings may be attributed to PO_4^{3-} groups, and a second O 1s peak at 532.8 eV is attributed to the contribution from the −OH group of HAP (Figures 6 and 7).[49]

As a result of XPS peak fitting, the C 1s spectrum, presented in Figures 6 and 7, consists of three components at positions 285.0, 286.6−287, and 288.0−289.3 eV, which are attributable to aromatic hydrocarbons and alkoxy and $RCOO^-$ groups, respectively.[50]

According to the literature, the C 1s peak with BE = 286−286.3 and 287.7−288.4 eV indicates the presence of carbonyl groups,[51] and the third deconvoluted peak, which occurred at 289.3 eV, corresponding to C−O bonds, suggests the presence of the polymer lignin, linked to the hydroxyapatite.

Finally, the titanium band positions (Ti 2p) in the XPS spectrum could not be deconvoluted and its chemical states could not be determined, since it is difficult to characterize a very thin Ti suboxide film.

The chemical composition of the outermost coating surface is important because it will be in direct contact with the bone tissue and dissolve first at the initial stage of implantation. It has been shown that the optimum Ca/P ratio is 1.67−1.76.[52] Thus, XPS analysis was used to determine the atomic Ca/P ratio of Ag/HAP and Ag/HAP/Lig coatings. The values of the Ca/P ratio of Ag/HAP and Ag/HAP/Lig coatings are shown in Table 2, where the increase of Ca/P confirms the HAP decomposition in the Ag/HAP coating after sintering, whereas the Ca/P ratio for the Ag/HAP/Lig coating remains constant and close to the stoichiometric value of 1.67.[52]

3.7. Electrochemical Impedance Spectroscopy. Electrochemical impedance spectroscopy (EIS) was used in order to study the corrosion stability of investigated coatings in the physiological environment such as the SBF solution. The Nyquist plots for the impedance of Ag/HAP and Ag/HAP/Lig coatings deposited on titanium as well as of thermally treated bare titanium as reference, after a prolonged exposure time in SBF solution at 37 °C, are presented in Figure 8, where the high-frequency range attributes to the coating, while the low-frequency range describes the characteristics of the passive oxide layer on titanium.

The fitting of experimental data obtained from Nyquist plots was accomplished by using the equivalent electrical circuits shown in Figure 9a,b, by the Gamry Instruments Echem Analyst fitting program. The equivalent circuits consist of the electrolyte resistance, R_s, the coating pore resistance, R_p, and constant phase elements, CPE_c and CPE_{pf}, which represent all the frequency-dependent electrochemical phenomena, such as the coating capacitance, C_c, and passive oxide film capacitance, C_{pf}. The fitting results are listed in Table 3.

The pore resistance, R_p, of Ag/HAP and Ag/HAP coatings is plotted as a function of time in Figure 10. It can be noticed that the pore resistance, R_p, and coating capacitance (data not shown) for both coatings remain almost constant over 10 days

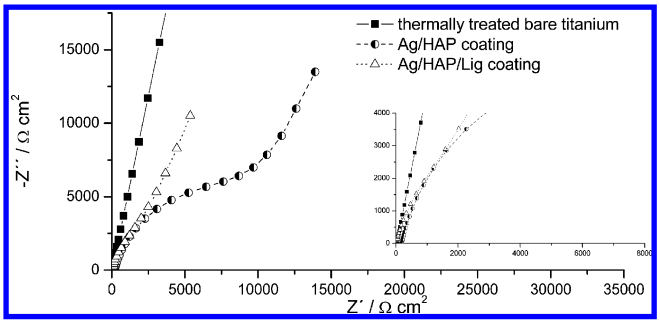

Figure 8. Nyquist plots of Ag/HAP and Ag/HAP/Lig coatings on titanium and thermally treated bare titanium after 10 days of exposure to SBF solution at 37 °C.

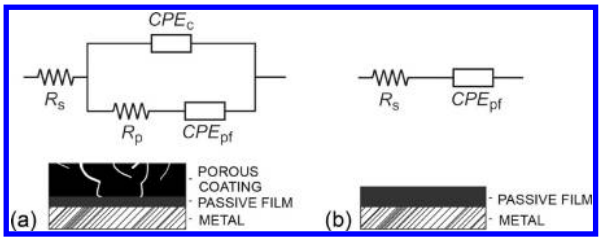

Figure 9. Equivalent electrical circuits and physical models for (a) Ag/HAP and Ag/HAP/Lig coatings on titanium and (b) thermally treated bare titanium during a prolonged exposure time to SBF solution at 37 °C.

of exposure to SBF solution, indicating the maintenance of good protective properties of the coatings. Furthermore, R_p values slightly increased and CPE_c slightly decreased for both coatings during the exposure of 10 days (Table 3), which has a direct relation with the amount of the apatite layer formed on the coating surfaces. The continuous increase in R_p and decrease in CPE_c reflect the process of the apatite nucleation after 1 week, which could also be clearly seen under SEM and FE-SEM observation (Figures 3 and 4, respectively), as well as from XRD and ATR-FTIR (Figures 2 and 5, respectively).

4. CONCLUSION

EIS was employed to show that both electrophoretically obtained Ag/HAP and Ag/HAP/Lig coatings provide good corrosion protection of titanium in SBF solution. Furthermore, a slight increase in coating pore resistance and a decrease in coating capacitance obtained by EIS during immersion for 240 h, as well as XRD, ATR-FTIR, XPS, SEM, and FE-SEM measurements, indicated the formation of a new phase, which means that both of the examined coatings exhibited effective biogrowth of hydroxyapatite during immersion in SBF, as demonstrated by a new crystalline, platelike structure surface formation, a property essential for bioactivity.

On the other hand, phase transformation of hydroxyapatite to other calcium phosphate phases after sintering at 900 °C was prevented by the presence of lignin in the composite Ag/HAP/Lig coating, which is confirmed by XRD, ATR-FTIR, and XPS results. The SEM and FE-SEM analyses have also indicated that the Ag/HAP/Lig coating had a more homogeneous, more compact, and less rough surface, while a lower value of contact angle in SBF, determined by the drop test, proved its better wettability, when compared to the Ag/HAP coating. On the basis of all results presented in this paper, it can be concluded that the Ag/HAP/Lig coating electrodeposited on titanium is a

dx.doi.org/10.1021/jp305252a | J. Phys. Chem. B 2013, 117, 1633−1643

Table 3. Fitting Values of Electrical Circuit Parameters

sample	time (h)	R_s (Ω cm^2)	CPE$_{pf}$ (μF cm^{-2})	n_{pf}	CPE$_C$ (μF cm^{-2})	n_C	R_p (kΩ cm^2)
Ag/HAP	24	65.3			223.4	0.88	6.6
	120	63.1			148.3	0.80	11.7
	240	85.6			123.0	0.85	12.6
Ag/HAP/Lig	24	29.2			627.2	0.88	5.6
	120	31.5			560.6	0.89	5.9
	240	21.8			543.5	0.88	6.3
thermally treated bare titanium	24	34.8	79.6	0.87			
	120	18.8	69.3	0.87			
	240	21.6	64.6	0.87			

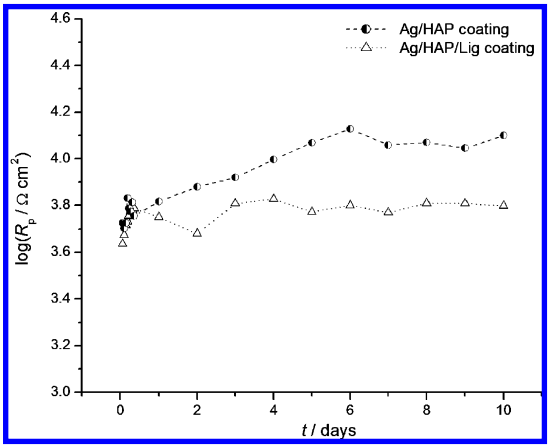

Figure 10. Time dependence of coating pore resistance, R_p, for Ag/HAP and Ag/HAP/Lig coatings during exposure to SBF solution at 37 °C.

promising candidate for the future development as a bioactive material.

AUTHOR INFORMATION

Corresponding Author

*Tel: +381 11 3303 737. Fax: +381 11 3370 387. E-mail:vesna@tmf.bg.ac.rs.

Notes

The authors declare no competing financial interest.

ACKNOWLEDGMENTS

This research was financed by the Ministry of Education and Science, Republic of Serbia, contracts Nos. III 45019 and III 45015, and by the National Sciences and Engineering Research Council of Canada (NSERC). A.J. was financed by the FP7 Nanotech FTM Grant Agreement 245916. The authors would like to thank Dr. Ljiljani Živković, Vinča Institute of Nuclear Sciences, University of Belgrade, for her help in PSD and ζ-potential measurements. We are also grateful to Mr. Yves Bédard, Département des Sciences du Bois et de la Forêt de l'Université Laval, for technical support and assistance in laboratory work, and to Mr. Alain Adnot, Université Laval, for his contribution to the XPS analysis.

REFERENCES

(1) Manivasagam, G.; Dhinasekaran, D.; Rajamanickam, A. *Recent Pat. Corros. Sci.* **2010**, *2*, 40−54.
(2) Wang, C. X.; Wang, M.; Zhou, X. *Langmuir* **2002**, *18*, 7641−7647.
(3) Garcia, C.; Cere, S.; Duran, A. *J. Non-Cryst. Solids* **2006**, *352*, 3488−3495.
(4) Kung, K.-C.; Lee, T.-M.; Lui, T.-S. *J. Alloys Compd.* **2010**, *508*, 384−390.
(5) Rath, P. C.; Besra, L.; Singh, B. P.; Bhattacharjee, S. *Ceram. Interfaces* **2012**, *38*, 3209−3216.
(6) Geetha, M.; Singh, A. K.; Asokamani, R.; Gogi, A. K. *Prog. Mater. Sci.* **2009**, *54*, 397−425.
(7) Swetha, M.; Sahithi, K.; Moorthi, A.; Srinivasan, N.; Ramasamy, K.; Selvamurugan, N. *Int. J. Biol. Macromol.* **2010**, *47*, 1−4.
(8) Pang, X.; Zhitomirsky, I. *Mater. Charact.* **2007**, *58*, 339−348.
(9) Mourino, V.; Cattalini, J. P.; Boccaccini, A. R. *J. R. Soc., Interface* **2012**, *9*, 401−419.
(10) Rameshbabu, N.; Sampath Kumat, T. S.; Prabhakar, T. G.; Sastry, V. S.; Murty, K. V. G. K.; Prasad Rao, K. *J. Biomed. Mater. Res., Part A* **2007**, *80*, 581−591.
(11) Lee, I.-S.; Whang, C.-N.; Oh, K.-S.; Park, J.-C.; Lee, K.-Y.; Lee, G.-H.; Chung, S.-M.; Sun, X.-D. *Nucl. Instrum. Methods Phys. Res., Sect. B* **2006**, *242*, 45−47.
(12) Pang, X.; Zhitomirsky, I. *Surf. Coat. Technol.* **2008**, *202*, 3815−3821.
(13) Simchi, A.; Tamjid, E.; Pishbin, F.; Boccaccini, A. R. *J. Nanomed. Nanotechnol.* **2011**, *7*, 22−39.
(14) Song, Y. W.; Shan, D. Y.; Han, E. H. *Mater. Lett.* **2008**, *62*, 3276−3279.
(15) Boccaccini, A. R.; Keim, S.; Ma, R.; Li, Y.; Zhitomirsky, I. *J. R. Soc., Interface* **2010**, *7*, 581−613.
(16) Corni, I.; Ryan, M. P.; Boccaccini, A. R. *J. Eur. Ceram. Soc.* **2008**, *28*, 1353−1367.
(17) Boccaccini, A. R.; Cho, J.; Subhani, T.; Kaya, C.; Kaya, F. *J. Eur. Ceram. Soc.* **2010**, *30*, 1115−1129.
(18) Kaya, C.; Singh, I.; Boccaccini, A. R. *Adv. Eng. Mater.* **2008**, *10*, 131−138.
(19) Stojanovic, D.; Jokic, B.; Veljovic, Dj.; Petrovic, R.; Uskokovic, P. S.; Janackovic, Dj. *J. Eur. Ceram. Soc.* **2007**, *27*, 1595−1599.
(20) Simović, K.; Mišković-Stanković, V. B.; Kićević, D.; Jovanić, P. *Colloids Surf., A* **2002**, *3209*, 47−55.
(21) Djošić, M. S.; Mišković-Stanković, V. B.; Janaćković, Dj. T.; Kačarević-Popović, Z. M.; Petrović, R. D. *Colloids Surf., A* **2006**, *274*, 185−191.
(22) Djošić, M. S.; Mišković-Stanković, V. B.; Kačarević-Popović, Z. M.; Jokić, B. M.; Bibić, N.; Mitrić, M.; Milonjić, S. K.; Jančić-Heinemann, R.; Stojanović, J. *Colloids Surf., A* **2009**, *341*, 110−117.
(23) Djošić, M. S.; Panić, V.; Stojanović, J.; Mitrić, M.; Mišković-Stanković, V. B. *Colloids Surf., A* **2012**, *400*, 36−43.
(24) Dong, X.; Dong, M.; Lu, Y.; Turley, A.; Jin, T.; Wu, C. *Ind. Crops Prod.* **2011**, *34*, 1629−1634.
(25) Gosselink, R. J. A.; Abächerli, A.; Semke, H.; Malherbe, R.; Käuper, P.; Nadif, A.; van Dam, J. E. G. *Ind. Crops Prod.* **2004**, *19*, 271−281.
(26) Fu, S. Z.; Guo, G.; Gong, C. Y.; Zeng, S.; Liang, H.; Luo, F.; Zhang, X. N.; Zhao, X.; Wei, Y. Q.; Qian, Z. Y. *J. Phys. Chem. B* **2009**, *113*, 16518−16525.
(27) Roy, N.; Bhowmick, A. K. *J. Phys. Chem. C* **2012**, *116*, 8763−8772.
(28) Baurhoo, B.; Ruiz-Feria, C. A.; Zhao, X. *Anim. Feed Sci. Technol.* **2008**, *144*, 175−184.

(29) Mansur, H. S.; Mansur, A. A. P.; Bicallho, S. M. C. M. *Key Eng. Mater.* **2005**, *284−286*, 745−748.
(30) Martinez, M.; Pacheco, A.; Vargas, M. *Rev. MVZ Córdoba* **2009**, *14*, 1624−1632.
(31) Erakovic, S.; Veljovic, Dj.; Diouf, P. N.; Stevanovic, T.; Mitric, M.; Milonjic, S.; Miskovic-Stankovic, V. B. *Int. J. Chem. React. Eng.* **2009**, *7*, A62.
(32) Wang, J.; De Boer, J.; De Groot, K. *J. Dent. Res.* **2004**, *83*, 296−301.
(33) Cai, K.; Frant, M.; Bossert, J.; Hildebrand, G.; Liefeith, K.; Jandt, K. D. *Colloids Surf., B* **2006**, *50*, 1−8.
(34) Wang, C.; Ma, J.; Cheng, W.; Zhang, R. *Mater. Lett.* **2002**, *57*, 99−105.
(35) Kim, J.-U.; Jeong, Y.-H.; Choe, H.-C. *Thin Solid Films* **2011**, *520*, 793−799.
(36) Wang, Y.; Zhang, X.; Yan, J.; Xiao, Y.; Lang, M. *Appl. Surf. Sci.* **2011**, *257*, 6233−6238.
(37) Vasilescu, C.; Drob, P.; Vasilescu, E.; Demetrescu, I.; Ionita, D.; Prodana, M.; Drob, S. I. *Corros. Sci.* **2011**, *53*, 992−999.
(38) Costa-Rodrigues, J.; Fernandes, A.; Lopes, M. A.; Fernandes, M. H. *Acta Biomater.* **2012**, *8*, 1137−1145.
(39) Ye, H.; Liu, X. Y.; Hong, H. *Mater. Sci. Eng., C* **2009**, *29*, 2036−2044.
(40) Siriphannon, P.; Kameshima, Y.; Yasumori, A.; Okada, K.; Hayashi, S. *J. Eur. Ceram. Soc.* **2002**, *22*, 511−520.
(41) Gu, Y. W.; Khor, K. A.; Cheang, P. *Biomaterials* **2004**, *25*, 4127−4134.
(42) Kim, H.-M.; Himeno, T.; Kokubo, T.; Nakamura, T. *Biomaterials* **2005**, *26*, 4366−4373.
(43) Pecheva, E. V.; Pramatarova, L. D.; Maitz, M. F.; Pham, M. T.; Kondyuirin, A. V. *Appl. Surf. Sci.* **2004**, *235*, 176−181.
(44) Ye, H.; Liu, X. Y.; Hong, H. P. *J. Mater. Sci.: Mater. Med.* **2009**, *20*, 843−850.
(45) Stoch, A.; Jastrzebski, W.; Brozek, A.; Trybalska, B.; Cichocinska, M.; Szarawara, E. *J. Mol. Struct.* **1999**, *511−512*, 287−294.
(46) Sun, R.; Li, M.; Lu, Y.; Wang, A. *Mater. Charact.* **2006**, *56*, 250−254.
(47) Wang, L.-N.; Luo, J.-L. *Mater. Sci. Eng., C* **2011**, *31*, 748−754.
(48) Roguska, A.; Pisarek, M.; Andrzejczuk, M.; Dolata, M.; Lewandowska, M; Janik-Czachor, M. *Mater. Sci. Eng., C* **2011**, *31*, 906−914.
(49) Yao, Z. Q.; Ivanisenko, Yu.; Diemant, T.; Caron, A.; Chuvilin, A.; Jiang, J. Z.; Valiev, R. Z.; Qi, M.; Fecht, H.-J. *Acta Biomater.* **2010**, *6*, 2816−2825.
(50) Watling, K. M.; Parr, J. F.; Rintoul, L.; Brown, C. L.; Sullivan, L. A. *Spectrochim. Acta A* **2011**, *80*, 106−111.
(51) Viornery, C.; Chevolot, Y.; Leonard, D.; Aronsson, B.-O.; Pechy, P.; Mathieu, H. J.; Descouts, P.; Gratzel, M. *Langmuir* **2002**, *18*, 2582−2589.
(52) Bai, X.; Sandukas, S.; Appleford, M. R.; Ong, J. L.; Rabiei, A. *Acta Biomater.* **2009**, *5*, 3563−3572.